

Accepted Manuscript

High temperature oxidation behavior of an equimolar refractory metal-based alloy 20Nb-20Mo-20Cr-20Ti-20Al with and without Si addition

B. Gorr, F. Mueller, H.-J. Christ, T. Mueller, H. Chen, A. Kauffmann, M. Heilmaier



PII: S0925-8388(16)32254-X

DOI: [10.1016/j.jallcom.2016.07.219](https://doi.org/10.1016/j.jallcom.2016.07.219)

Reference: JALCOM 38388

To appear in: *Journal of Alloys and Compounds*

Received Date: 15 January 2016

Revised Date: 15 July 2016

Accepted Date: 20 July 2016

Please cite this article as: B. Gorr, F. Mueller, H.-J. Christ, T. Mueller, H. Chen, A. Kauffmann, M. Heilmaier, High temperature oxidation behavior of an equimolar refractory metal-based alloy 20Nb-20Mo-20Cr-20Ti-20Al with and without Si addition, *Journal of Alloys and Compounds* (2016), doi: 10.1016/j.jallcom.2016.07.219.

This is a PDF file of an unedited manuscript that has been accepted for publication. As a service to our customers we are providing this early version of the manuscript. The manuscript will undergo copyediting, typesetting, and review of the resulting proof before it is published in its final form. Please note that during the production process errors may be discovered which could affect the content, and all legal disclaimers that apply to the journal pertain.

High Temperature Oxidation Behavior of an Equimolar Refractory Metal-based Alloy 20Nb-20Mo-20Cr-20Ti-20Al with and without Si Addition

B. Gorr^{a*}, F. Mueller^a, H.-J. Christ^a, T. Mueller^b, H.Chen^c, A. Kauffmann^c, M. Heilmaier^c

^a*Institut für Werkstofftechnik, Universität Siegen, Paul-Bonatz-Str. 9-11, 57068 Siegen, Germany*

^b*Institut für Bau- und Werkstoffchemie, Universität Siegen, Paul-Bonatz-Str. 9-11, 57068 Siegen, Germany*

^c*Institut für Angewandte Materialien - Werkstoffkunde (IAM-WK), Karlsruhe Institute of Technology (KIT), Engelbert-Arnold-Str. 4, D-76131 Karlsruhe, Germany*

*Corresponding author: Email: gorr@ifwt.mb.uni-siegen.de; phone: +492717404653

Abstract

The high temperature oxidation behavior of a refractory high-entropy alloy (HEA) 20Nb-20Mo-20Cr-20Ti-20Al at 900°C, 1000°C and 1100°C was investigated. The oxidation kinetics of the alloy was found to be linear at all temperatures. Oxide scales formed are largely inhomogeneous showing regions with thick and porous layers as well areas with quite thin oxide scales due to formation of discontinuous chromium-rich oxide scales. However, the oxidation resistance can be moderately improved by the addition of 1 at.% Si. The thermogravimetric data obtained during oxidation of the Si-containing alloy at 1000°C and 1100°C reveal pronounced periods of parabolic oxidation that, however, change towards linear oxidation after prolonged exposure times. Microstructural investigations using scanning electron microscopy (SEM) and transmission electron microscopy (TEM) document that the Si addition gives rise to a nearly continuous alumina-rich layer which seems to be responsible for the good protection against further oxidation. Pronounced zones of internal corrosion attacks consisting of different oxides and nitrides were observed in both alloys. In order to determine the chemical composition of the corrosion products and their mass fraction, quantitative X-ray diffraction (XRD) analysis was performed on powdered oxide scales that formed on the alloys after different oxidation times. Rutile was identified as the major phase in the oxide scales rationalizing the relatively high mass gain during oxidation.

1. Introduction

Equiatomic multicomponent alloys have attracted great attention among material scientists worldwide in the last few years [1,2] due to their unique properties. Regarding the microstructure, HEAs stand out due to their tendency to possess simple, highly symmetric crystal structures, which often lead to single-phase microstructures [3], to nanoparticles in the matrix [4] and to sluggish diffusion of elements [5-7]. High temperature stability was reported by Hsieh et al. and Liu et al. for the alloy systems AlCrFeMnNi and FeCoNiCrMn, respectively [8, 9]. With respect to mechanical properties, the so-called Cantor alloy sticks out in having simultaneously high strength and ductility, both of which increase with decreasing temperature [10, 11]. Refractory HEAs exhibit extremely high strength at elevated temperatures exceeding even the levels provided by advanced Ni-based superalloys [12].

Characterization of the oxidation resistance of the alloy AlSiTiCrFeCoNiMo_{0.5} and AlSiTiCrFeNiMo_{0.5} was in part studied by Huang et al. who mainly focused on processing, microstructure, and wear resistance of the alloys [13]. It was concluded that the formation of the chromia-based layer underneath the outermost titanium oxide scale accounts for the good oxidation resistance of these materials. Daoud et al. characterized the oxidation behavior of three alloys based on the alloy system Al-Co-Cr-Cu-Fe-Ni [14]. Thin layers of α -Al₂O₃ and Cr₂O₃ were identified after 200h of oxidation at 1000°C, however severe spallation of oxide scales was also observed. High

temperature oxidation behavior of multicomponent alloys of the system Al-Co-Cr-Ni-(Fe or Si) was investigated by Butler et al. [15]. They found that the formation of the external alumina is strongly dependent on the Al content in the alloys. The oxidation behavior of other transition metal-based HEAs has been frequently reported in the literature [16-21]. By contrast, there is a pronounced lack of studies dealing with high temperature oxidation behavior of refractory metal-based HEAs, despite the fact that these materials have been designed for high temperature applications. Senkov et al. investigated oxidation resistance of a refractory HEA NbCrMo_{0.5}Ta_{0.5}TiZr in flowing air at 1000°C [22]. A scale consisting of complex oxides was found on the alloy surface. Nevertheless, the alloy exhibits a much better combination of mechanical properties and oxidation resistance than commercial Nb alloys as well as NbSiAlTi and NbSiMo materials [22]. The study by Liu et al. revealed that the oxidation rates of refractory HEAs is significantly decreased by Ti and Si additions, while V additions cause on the contrary increased oxidation rates at 1300°C [23]. The properties of HEAs as protective coating have also been investigated. The oxidation resistance of the alloy Ti-6Al-4V could be improved due to the laser clad TiVCrAlSi high entropy alloy coatings [24].

The equiatomic alloy 20W-20Mo-20Cr-20Ti-20Al is the first material from the recently proposed new alloy family that has been developed for high temperature structural applications [25]. Since W and Mo possess very high melting points, these elements were considered as prime candidates for the new alloy system. To possibly enable the formation of a protective oxide scale, Cr and Al were added to the alloy system, while Ti should reduce the alloy density. Further details regarding the alloy design concept can be found in [25]. Microstructure analysis of the alloy 20W-20Mo-20Cr-20Ti-20Al in the as-cast condition as well after annealing at high temperatures revealed that the alloy shows a clear tendency to homogenize yielding a simple single-phase body centered cubic (BCC) microstructure [26]. The microstructure and mechanical properties of the second alloy of this family, 20Nb-20Mo-20Cr-20Ti-20Al, were presented and discussed by Chen et al. [27] whereby tungsten has been replaced by niobium to further reduce density and to ease the fabrication by arc melting due to the lower melting point of Nb. The purpose of the present paper is twofold: (a) to assess the high temperature oxidation behavior of the equiatomic HEA 20Nb-20Mo-20Cr-20Ti-20Al and (b) to study the effect of 1 at.% of the Si addition aiming at enhancing the oxidation resistance following the recommendation by [23].

2. Experimental

The alloys were produced from elemental bulk materials by arc-melting in ~0.6 atm of argon (arc-melter AM 0.5 by Edmund Bühler GmbH). The purities of the starting materials Mo, Nb, Al, Cr, Ti, and Si were 99.9%, 99.9%, 99.9%, 99%, 99.8% and 99.9999%, respectively. Nitrogen impurities were found to be below the detection limit, oxygen content was measured being between 50 and 100 wt. ppm. The prepared buttons were flipped over and remelted more than five times in a water-chilled copper mold to facilitate alloy homogenization. The alloys were heat-treated under Ar flow for 20h at 1200°C. For the oxidation tests, samples of dimension of approximately 10 mm x 10 mm x 2 mm were polished up to 1000 grit. The samples were ultrasonically cleaned in ethanol directly before testing in a Rubotherm thermogravimetric system. The oxide scale morphology was analyzed by means of a FIB-SEM DualBeam system of type FEI Helios Nanolab 600 equipped by the energy dispersive X-ray (EDX) detector. Before cross-section analysis, oxidized samples were Ni-plated to protect the oxide scales. A TEM-lamella was prepared applying ion milling in the FIB-SEM system. TEM analysis was performed in the TEM of type FEI Talos F200X. To analyze the composition of oxides formed on the alloys, XRD measurements were carried out using the X'Pert Pro MPD diffractometer (Cu-K α radiation) operating with Bragg-Brentano geometry. Divergence slits 1/2 degree and anti scatter slit 1 degree were used for XRD measurements. Oxide scales were removed from the oxidized samples

and powdered into particle sizes smaller than 40 μm . Since the oxide scales were relatively thin, particularly after short oxidation experiments, background-free sample holders made of silicon single crystals (Panalytical PW 1817/32) were used. The measurements were carried out using 2θ angles between 10 and 78° , the step size was adjusted to $0,017^\circ$, the scan time for a step was 30s. In order to quantify the amount of phases formed during oxidation, Rietveld analysis was performed using the cif-files (anatase (ICSD9852) [28], corundum (ICSD 160604 [29]), and rutile (ICSD 9161) [30]). The values of the standard free energy of formation of oxides and nitrides were calculated using the software FactSage V6.4 in conjunction with the SGPS database.

3. Results

3.1 Oxidation kinetics

Figure 1(a) shows thermogravimetric curves observed during exposure of the alloy Nb-Mo-Cr-Ti-Al to laboratory air at 900°C, 1000°C and 1100°C. The curves obtained at 900°C and 1000°C obviously obey the linear oxidation kinetics, whereby the oxidation rate at 1000°C is substantially higher compared to that at 900°C indicating formation of non-protective oxide scales. Oxidation kinetics at 1100°C shows a tendency to become decelerated after approximately 25h of air exposure. The total mass gain after 48h of oxidation at 1100°C is slightly lower compared to that at 1000°C. It can be assumed that the oxide scale formed on the alloy Nb-Mo-Cr-Ti-Al at 1100°C becomes at least partially protective after prolonged oxidation times.

Thermogravimetric curves of the alloy Nb-Mo-Cr-Ti-Al-1Si obtained during oxidation at the same temperatures as for the Si-free alloy are shown in Fig. 1(b). The alloy oxidizes according to the linear rate law at 900°C, while the thermogravimetric curves for 1000°C and 1100°C apparently show an initially parabolic weight gain which changes to the linear rate law after approximately 30h. The oxidation kinetics at 1100°C is only slightly higher compared to that at 1000°C. The first few hours of transient oxidation are usually characterized by rapid oxidation of all elements present in the alloy. After a period of parabolic oxidation, an effect similar to breakaway oxidation, i.e. the oxidation rate increases markedly approaching the linear mass gain, is observed for the Si-containing alloy at 1000°C and 1100°C. This effect correlates with a change in the scale structure during oxidation towards formation of thick, porous oxide scales accompanied by enhanced ingress of gaseous species down to the metal phase. This will be discussed in more detail below. Given the high fraction of refractory elements contained in the HEAs studied, the weight gains found after nearly 50 hours are relatively low (below 10 mg/cm^2).

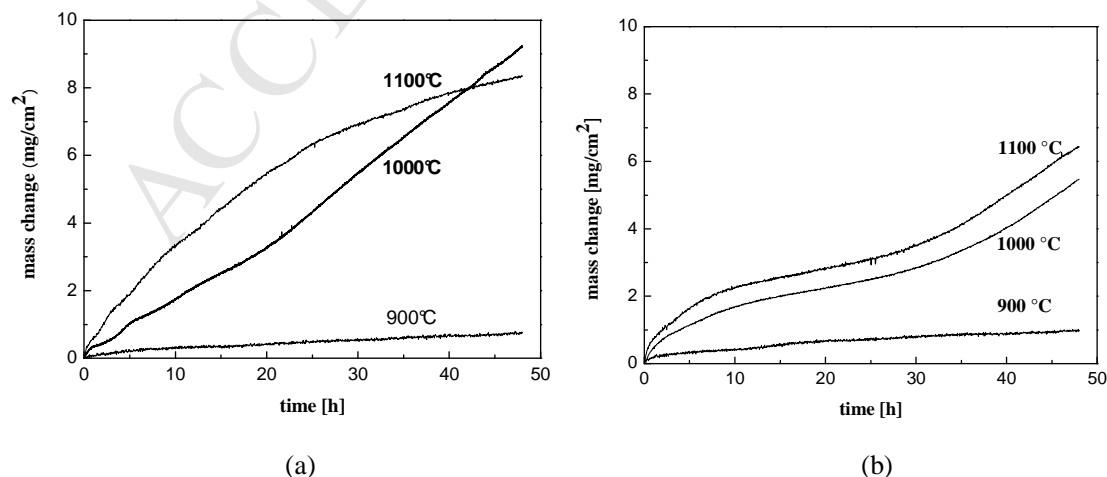
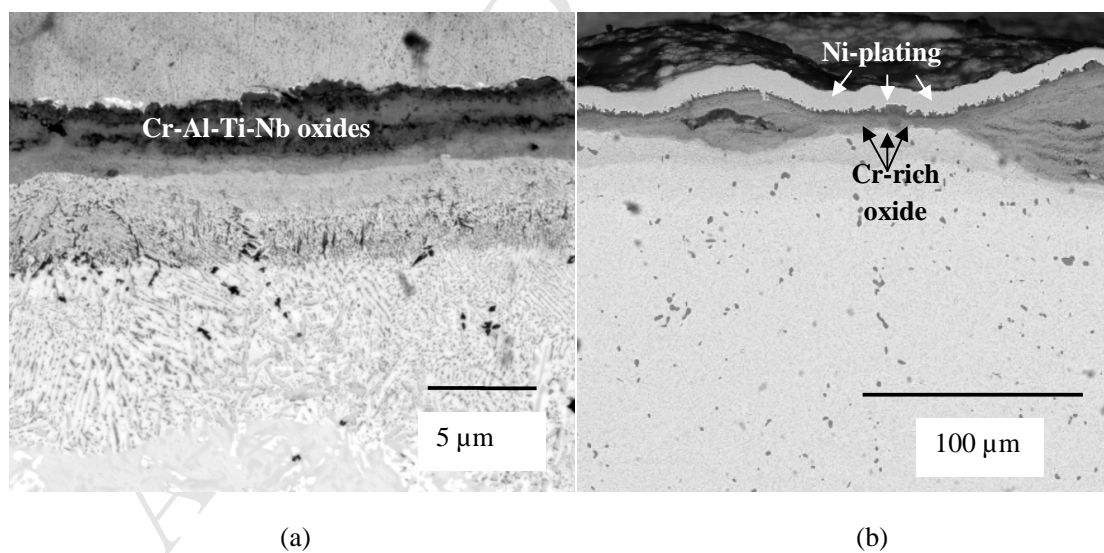


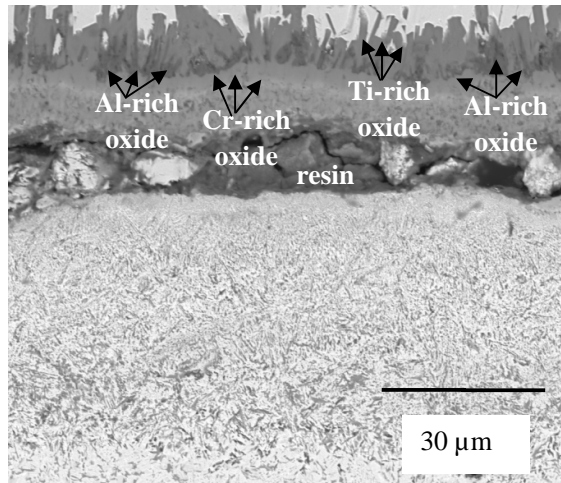
Figure 1: Oxidation kinetics of alloys (a) Nb-Mo-Cr-Ti-Al and (b) Nb-Mo-Cr-Ti-Al-1Si

3.2. Microstructural analysis of oxide scales

3.2.1. Alloy Nb-Mo-Cr-Ti-Al

The oxide scale formed on the alloy Nb-Mo-Cr-Ti-Al at 900°C after 48h of oxidation is shown in Fig. 2(a). The scale is largely homogeneous and is approximately 4 μm thick. The EDX analysis of the oxide scale (not shown here) reveals that the scale consists of a mixture of Ti, Al, Cr, and Nb oxides. Such oxide layers are non-protective in nature and thus can explain the linear oxidation at 900°C (see Fig. 1(a)). Figure 2(b) shows the morphology of the oxide scale formed on the alloy Nb-Mo-Cr-Ti-Al after 48h of oxidation at 1000°C. Two different kinds of oxide morphology can be observed: (i) a thick (up to $\sim 80\mu\text{m}$) and porous oxide mixture and (ii) a relatively thin (up to $\sim 15\mu\text{m}$) and compact oxide layer. EDX analysis (not shown here) of these two distinctive regions revealed that Ti, Al, Cr and Nb, i.e. their oxides, are nearly homogeneously distributed in the thick oxide layers, while a discontinuous Cr oxide-rich layer was identified within the oxide scale in the case of the thin oxide layer. Interestingly, enrichment of Mo was found at the interface oxide/substrate indicating that evaporation of Mo oxides can be neglected. At 1100°C, the microstructure of the oxide scale changes significantly compared to that formed at the lower temperatures. The oxide scale is mostly homogeneous and is about 25 μm thick (see Fig. 2(c)). Underneath the coarse crystals of Ti oxide clearly visible in the outermost part of the scale, a semi-continuous Al oxide-rich layer can be identified. The decelerated oxidation kinetics at 1100°C can apparently be attributed to the formation of this Al oxide-rich layer. However, the microstructural analysis of the cross-sections after discontinuous oxidation tests revealed that the Al oxide-rich scale could only be detected after a prolonged oxidation time, i.e. after at least 24h. Further, a continuous Cr oxide-rich layer was observed underneath the Al oxide-rich scale that also contributes to slowing down the kinetics (see Fig. 2(c)). Underneath the Cr oxide-rich scale, Ti and Nb oxides were identified to prevail. It should also be mentioned that some areas with the thick scale similar to that formed at 1000°C were predominantly located on sample corners.

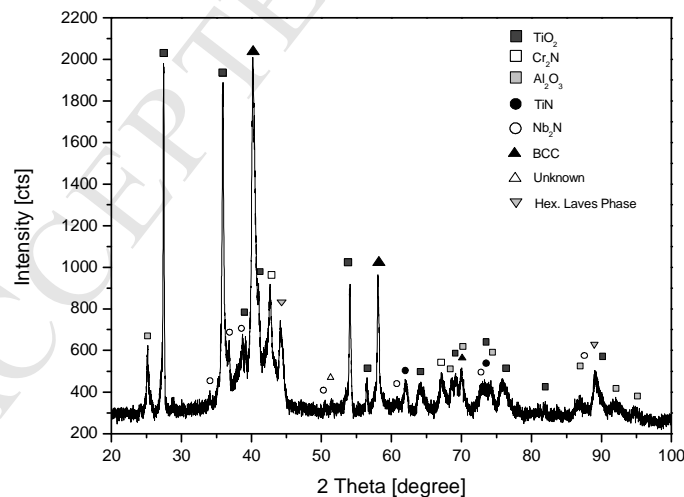




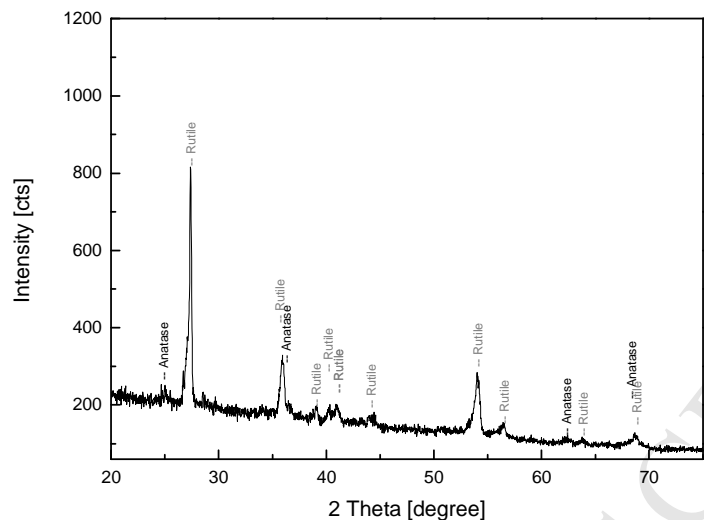
(c)

Figure 2: Cross-section (BSE) of the alloy Nb-Mo-Cr-Ti-Al after 48h oxidation at (a) 900°C, (b) 1000°C, and (c) at 1100°C

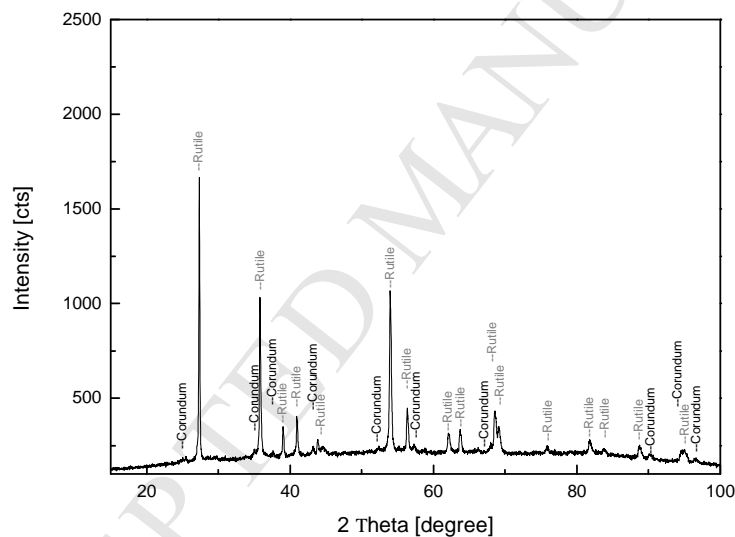
As shown in Figs. 2 (a)-(c), thick zones of internal precipitates were found underneath the oxide scales. In order to analyze these precipitates, the oxide scale was completely ground off from the sample oxidized for 48h at 1000°C, and a XRD measurement was carried out on the metallic substrate containing the internal precipitates. The results are shown in Fig. 3. The metallic substrate consists of the major solid solution BCC phase, the minor Laves phase (Cr_2Nb) as well as an unknown phase. These findings are in agreement with previous investigations of the alloy microstructure [27]. In addition to the very stable oxides, i.e. Al_2O_3 and TiO_2 , three types of nitrides were detected: TiN , Cr_2N and a Nb_2N . Considering the rather thick zone of internal precipitates, it can be concluded that the alloy Nb-Mo-Cr-Al-Ti is extremely susceptible to nitrogen ingress.



(a)



(b)



(c)

Figure 3: XRD patterns of (a) the zone with internal precipitates formed underneath the oxide scale on the alloy Nb-Mo-Cr-Ti-Al after 48h oxidation at 1000°C, (b) powdered oxide scales formed on the alloy Nb-Mo-Cr-Ti-Al after 8h oxidation at 1000°C and (c) powdered oxide scales formed on the alloy Nb-Mo-Cr-Ti-Al after 48h oxidation at 1000°C

To identify the nature of corrosion products formed in the outermost scale and to estimate the amounts of different oxides as a function of the oxidation time, the oxide scales were removed from the samples oxidized for 8h, 24h and 48h in air at 1000°C, crushed into powders and quantitatively analyzed using XRD. Figure 3 (b) and (c) shows the XRD patterns of the powdered oxide scales formed on the alloy Nb-Mo-Cr-Ti-Al at 1000°C after 8h and 48h of exposure, respectively. The results are summarized in Table 1. Three crystal structures were identified, namely, rutile, corundum, and anatase. For all oxidation times, rutile seems to be the prevailing phase. The high amount of rutile can clearly be related to the formation of TiO_2 that was confirmed by the EDX analysis. However, Nb_2O_5 exhibits polymorphism and can also crystallize in the rutile (TiO_2) structure [31]. Furthermore,

Novotny reported that solubility of Nb_2O_5 in TiO_2 varies between 2 at.% and 41 at.% [32]. Besides, Nb oxide was identified by the EDX analysis of the oxide scale. Therefore, the two oxides TiO_2 and Nb_2O_5 can be responsible for the presence of rutile in the scale formed on the alloy Nb-Mo-Cr-Ti-Al. The negligibly small amount of anatase was only found after 8h of oxidation. The two oxides Al_2O_3 and Cr_2O_3 that can form in this alloy during oxidation, possess the crystal structure of corundum. Bondioli et al. reported that below 950°C a miscibility gap forms, where Al_2O_3 and Cr_2O_3 coexist, while above this temperature complete miscibility is present [33].

Table 1: Phase fractions of corrosion products after oxidation of the alloy Nb-Mo-Cr-Ti-Al at 1000°C

Oxidation time	8h	24h	48h
Rutile, %	98.4	88.3	84.5
Corundum, %	-	11.7	15.5
Anatase %	1.6	-	-

Results of the thermogravimetric analysis shown in Fig. 1b clearly demonstrate that Si has a beneficial effect on the oxidation behavior of the alloy Nb-Mo-Cr-Ti-Al. In literature, numerous studies exist suggesting several hypotheses on the positive effect of Si with respect to high temperature oxidation resistance [34, 35]. The two most commonly accepted ones are: (i) depending on the alloy system, Si favors the formation of either a protective external silica scale or of a silica layer on the phase boundary oxide/alloy [36] and (ii) SiO_2 acts as nucleation sites promoting the rapid formation of a continuous protective layer [37, 38]. In order to proof hypothesis (ii), on one side of the samples of the alloy Nb-Mo-Cr-Ti-Al a thin (~ 20 nm) SiO_2 layer was sputter deposited, while the other side remained untreated. The sample was subsequently oxidized in air for 48h at 1000°C . As shown in Fig. 4, no difference can be identified between the sputtered and non-sputtered sides of the sample. It can, thus, be concluded that SiO_2 sputter deposition does not lead to a noticeable improvement of the oxidation resistance of the alloy Nb-Mo-Cr-Ti-Al. The fast growing oxide mixture clearly governs the entire oxidation process suppressing or even eliminating the possible positive Si effect from the formation of nucleation sites.

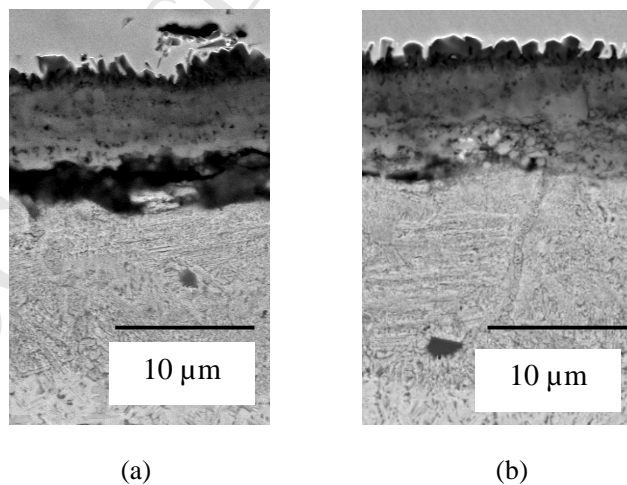


Figure 4: Effect of SiO_2 sputter deposition on the oxidation behavior of the alloy Nb-Mo-Cr-Ti-Al after 48h of oxidation at 1000°C ; (a) sputtered side of the oxidized samples, (b) non-sputtered side of the oxidized samples (BSE-images)

3.2.2. Alloy Nb-Mo-Cr-Ti-Al-1Si

Figures 5(a)-(c) show the cross-sections of the alloy Nb-Mo-Cr-Ti-Al-1Si after 48h of exposure to air at 900°C, 1000°C, and 1100°C. Similar to the case of the Si-free alloy, the oxide scale formed on the Si-containing alloy at 900°C is approximately 4 μm thick and represents a mixture of Ti, Al, Cr, and Nb oxides. The main parts of the oxide scales formed at 1000°C and 1100°C are 7 μm and 20 μm thick, respectively. Thicker and more porous oxide scales, if present, were occasionally observed on the sample corners (see Fig. 5(d)). Obviously, the dramatic increase in the oxidation rate after approximately 30h of oxidation, Fig. 1(b), can be attributed to the formation of these thick layers on the sample corners.

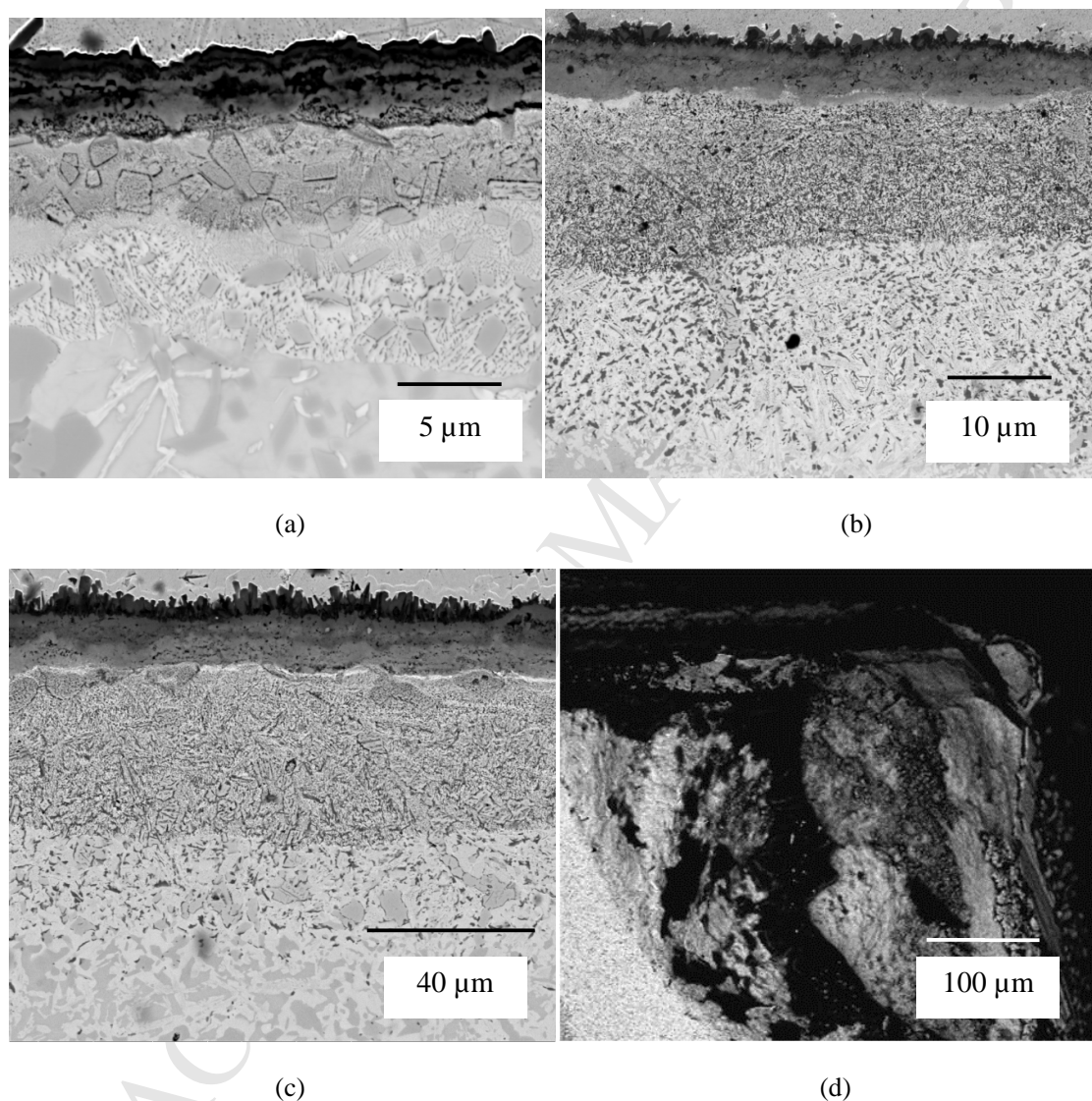
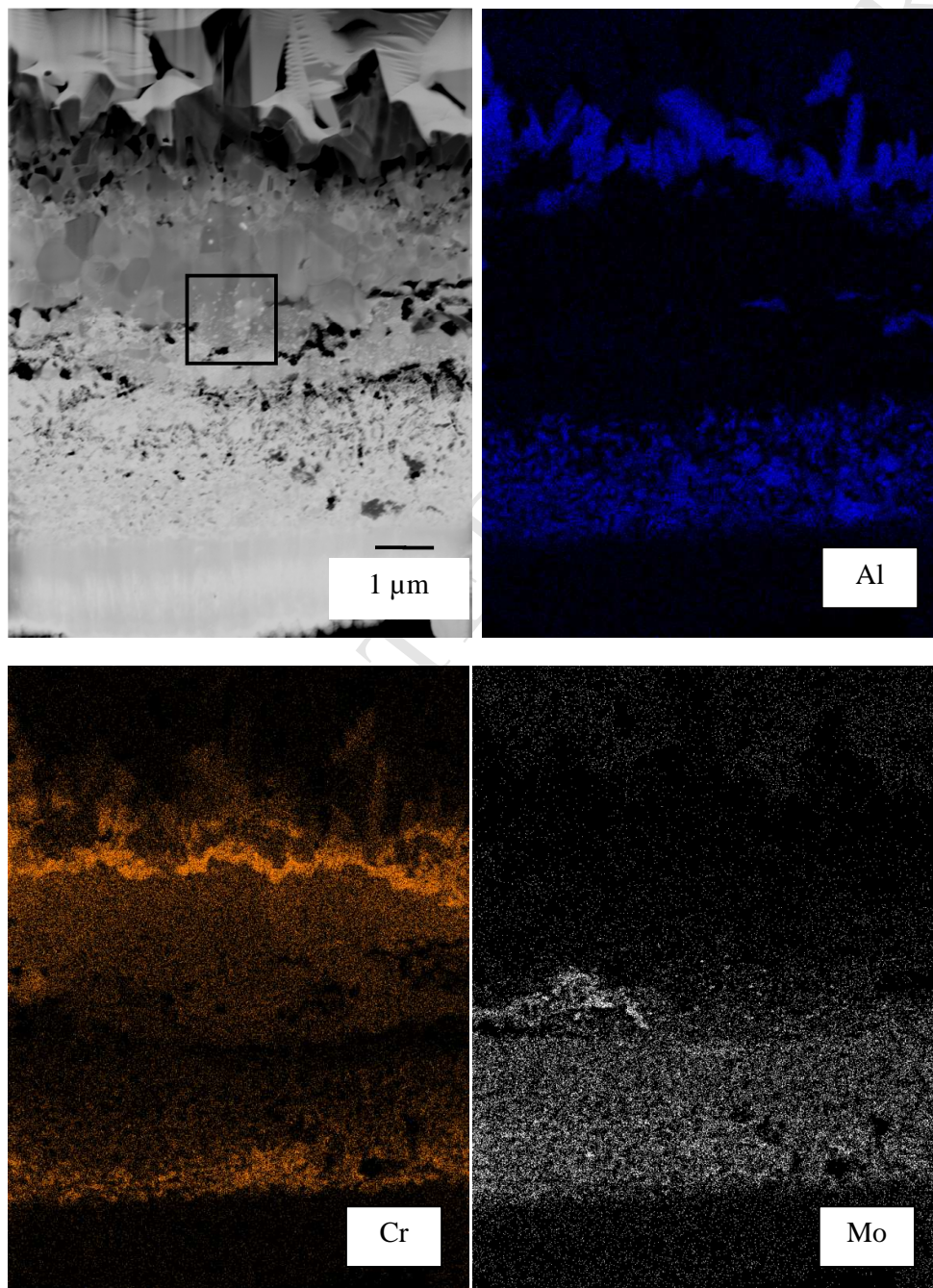


Figure 5: Cross-section (BSE) of the alloy Nb-Mo-Cr-Ti-1Si after 48h oxidation at (a) 900°C, (b) 1000°C, and (c) at 1100°C; (d) corner of the oxidized sample Nb-Mo-Cr-Ti-1Si at 1100°C

In order to get a deeper insight into the morphology of the oxide scales formed at higher temperatures, a TEM lamella was prepared using ion milling in the SEM-FIB device from a sample oxidized at 1000°C for 48h. The morphology of the oxide layer and corresponding results of EDX analyses carried out in TEM are shown in Fig. 6. These results clearly reveal that nearly continuous Al oxide- and Cr oxide-rich scales are formed underneath coarse Ti oxide grains. The moderate mass gain during oxidation of the alloy Nb-Mo-Cr-Ti-Al-1Si at 1000°C and 1100°C for up to 30 h can be explained by

the formation of these oxide layers. Still as for the base alloy described in the previous section, a significant amount of Nb and Ti oxides was also observed in the oxide scale. The distribution of Nb in the oxide scale indicates that the Al oxide-rich scale is the only efficient barrier against Nb diffusion since Niobium was detected exclusively underneath the Al-rich oxide layer. Another important positive finding is that Mo was only detected in the metallic substrate suggesting that the evaporation of Mo oxides can be largely excluded. Results of the EDX analysis of the zone marked in Fig. 6 as a black frame revealed that the small bright particles at the interface oxide/substrate consists of nearly pure Mo (see the magnified view of Fig. 6a in Fig. 7 together with the element specific mapping of molybdenum and oxygen). In addition, a pronounced zone of internal precipitates can clearly be seen in Figs. 5 and 6. These internally precipitated corrosion products are supposed to be the same as the ones identified in the previous section for alloy Nb-Mo-Cr-Ti-Al.



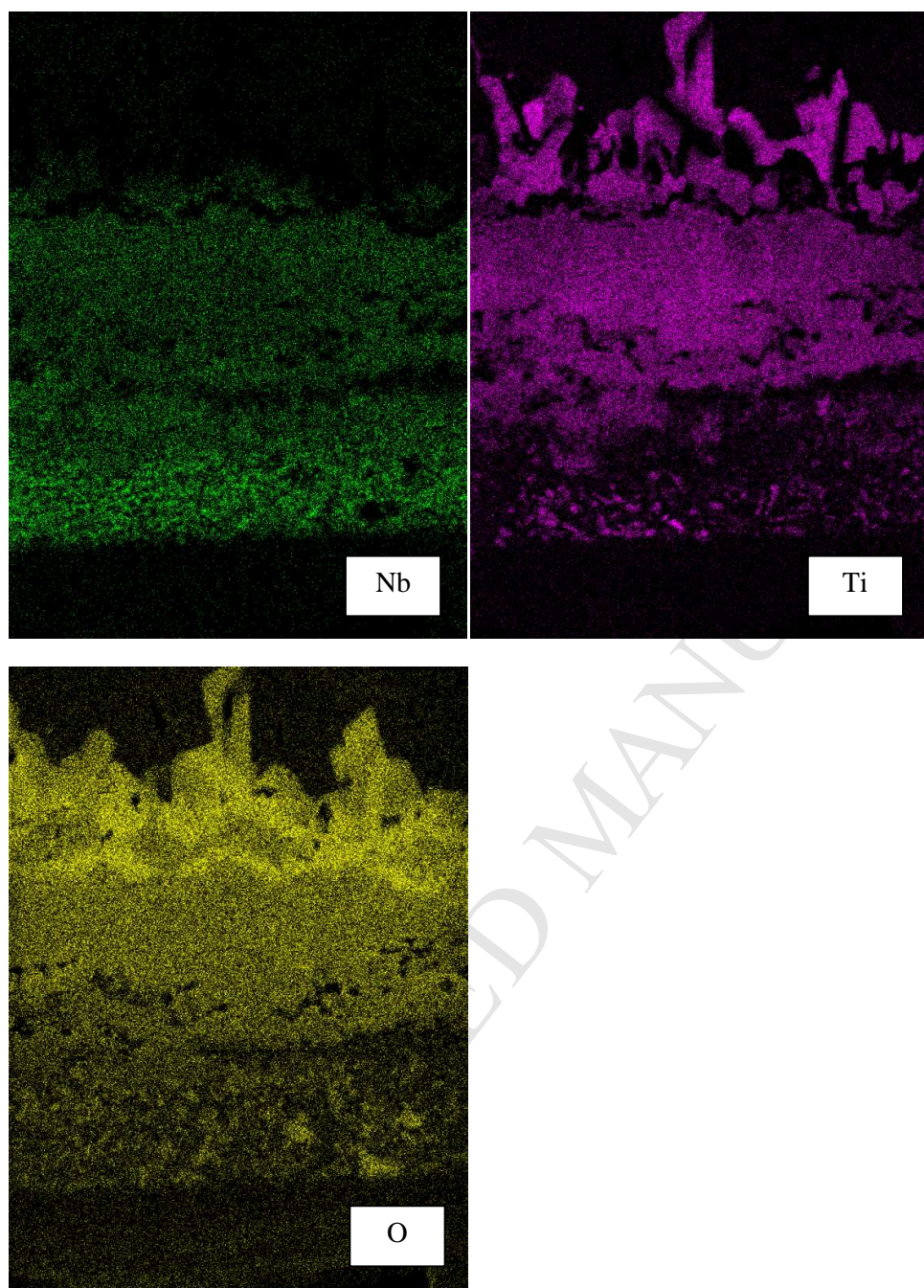


Figure 6: TEM-bright field micrograph of a cross-section through the oxide scale of the alloy Nb-Mo-Cr-Ti-Al-1Si after 48h oxidation at 1000°C and the corresponding element-specific EDX mappings. The black box indicated in the bright field micrograph is presented as an enlarged view in Fig. 7.

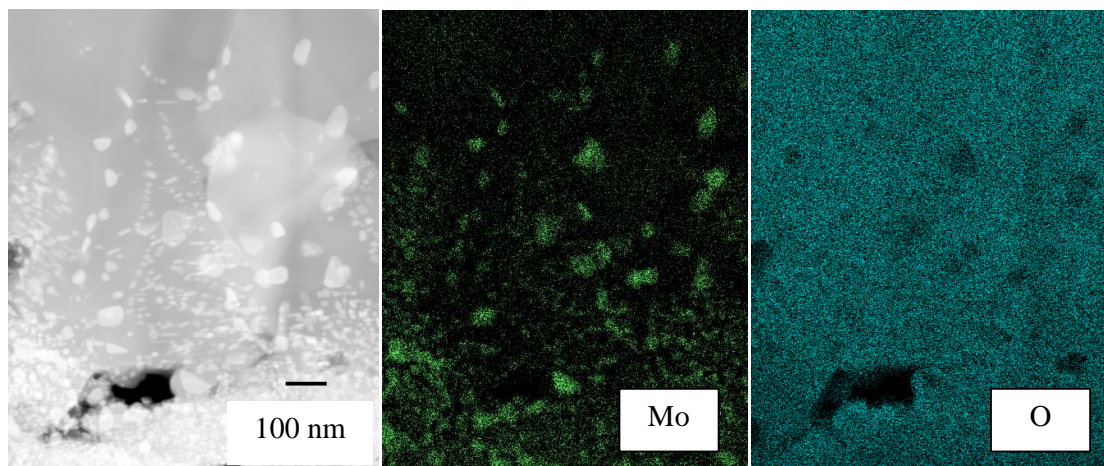


Figure 7: EDX analysis of the zone marked in Fig. 6

The results of the quantitative XRD analysis (prepared in the same way as described above for the Si-free alloy) of corrosion products after oxidation of the alloy Nb-Mo-Cr-Ti-Al-1Si at 1000°C are summarized in Table 2. Figure 8 shows exemplarily the XRD patterns of the powdered oxide scale formed during 24h of oxidation at 1000°C. It was found that only two crystal structures are present after both 24h and 48h air exposure, namely rutile and corundum. No anatase could be detected, though. Different to the Si-free alloy, the amount of the oxide powder available after 8h of oxidation was too small to carry out XRD measurements. The rutile phase is again the major phase of the corrosion products formed on the alloy Nb-Mo-Cr-Ti-Al-1Si. The phase fraction of rutile increases slightly with oxidation time, while the percentage of corundum decreases correspondingly. The observed increase of the oxidation rate after 30h of oxidation (see Fig. 1(b)) is an indication that the alumina and/or chromia scale loses its protectiveness, especially at the sample corners, causing the enhanced formation of fast growing and non-protective rutile.

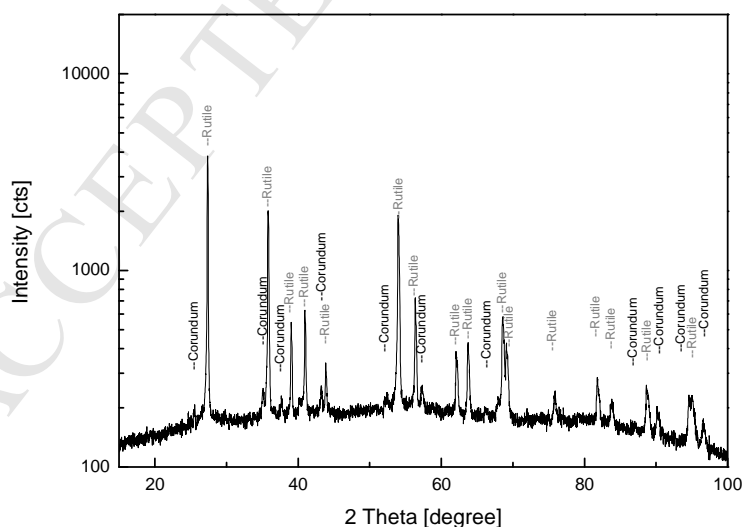


Figure 8: XRD patterns of the powdered oxide scale formed on the alloy Nb-Mo-Cr-Ti-Al-1Si after 24h of oxidation at 1000°C

Table 2: Phase fraction of corrosion products after oxidation of the alloy Nb-Mo-Cr-Ti-Al-1Si

Oxidation time	24h	48h
Rutile, %	89.7	93.2
Corundum, %	10.3	6.8

4. Discussion

The experimental results presented in the previous section reveal a moderately beneficial effect of the Si addition on the oxidation behavior of the equiatomic alloy Nb-Mo-Cr-Ti-Al. Comparing the thermogravimetric curves of the Si-free and Si-containing alloy, it can be concluded that the better oxidation resistance at 1000°C and 1100°C of the alloy Nb-Mo-Cr-Ti-Al-1Si manifests itself (i) in a lower values of the total mass gain after 48h of air exposure compared to the Si-free alloy and (ii) in an interim period of parabolic oxidation. However, at 900°C, the thermogravimetric results of both alloys are rather similar. The microstructural analyses of the oxide scales formed on both alloys at 900°C reveal this resemblance in the oxide thickness and the constitution of the oxide layers. These oxide scales represent a non-protective mixture of various oxides explaining the linear mass gain at 900°C. At higher temperature, however, the constitution of the oxides scales formed on both alloys substantially differs. While the oxide scale of the Si-free alloy includes only a partly continuous Cr oxide-rich scale at 1000°C and an additional semi-continuous Al oxide-rich scale that forms after a prolonged oxidation time at 1100°C, the alloy Nb-Mo-Cr-Ti-Al-1Si forms both, Cr oxide- and Al oxide-rich layers, at 1000°C as well as at 1100°C that are also noticeably more dense and compact compared to those formed on the Si-free alloy. Thus, it can be concluded that the formation of an Al oxide-rich scale in the alloy system Nb-Mo-Cr-Ti-Al is promoted by higher temperatures, prolonged oxidation time as well as Si additions. It should, however, be pointed out that the sample surfaces of both alloys after oxidation at 1000°C and 1100°C are covered by a non-uniform oxide scale showing regions of a thick, non-protective and quickly growing scale as well as regions with a relatively thin, to some extent protective oxide scale due to the formation of the Cr oxide-rich and Al oxide-rich layers mentioned above. The thick and non-protective scale seems to form at random on the alloy Nb-Mo-Cr-Ti-Al, while on the alloy Nb-Mo-Cr-Ti-Al-1Si it appears predominantly on the sample corners. It is well-known that oxide scales are less adherent on convex surfaces, e.g. corners of specimens, than on flat or concave surfaces because of the high tensile stresses developing in the growing scale [39]. As a consequence of these stresses, porosity and microchannels form in the scale resulting in the loss of protectiveness primarily on the specimen corners [39]. For the alloy Nb-Mo-Cr-Ti-Al-1Si it can, hence, be concluded that an effect similar to the breakaway oxidation, i.e. the local formation of thick and fast growing scales after a certain period of oxidation, takes place explaining the increase of the oxidation rate after 30h of oxidation at 1000°C and 1100°C. The general reason why the Si-containing alloy shows a better oxidation behavior compared to that of the Si-free alloy is still unclear as the coverage of the alloy surfaces by a thin sputtered SiO₂ layer that should promote the formation of protective oxide scales did not show an appreciable effect on the oxide scale formation at least after longer oxidation times. A possible explanation of the positive effect of Si addition would be that Si favorably increases the activities of Cr and/or Al in the alloy, hence, leading to a higher driving force for the formation of the protective oxides Cr₂O₃ and Al₂O₃. The thermodynamic effect of Si in the alloy system studied will, thus, be explored in a future investigation in detail.

The mass fractions of oxides observed using XRD and their evolution during oxidation can be discussed only qualitatively, i.e. in terms of the major phase, minor phases and traces, and, therefore, cannot be unambiguously correlated with other experimental results, such as the thermogravimetric data. The reason for this restriction is that the phase fractions were determined assuming that rutile is represented by TiO₂ and corundum by Al₂O₃. The EDX results, however, show that other oxides are also extensively present in the oxide scales and possess the same crystal structures, which for instance

holds true for Cr_2O_3 and Al_2O_3 . A comparison of the oxide mass fraction differences between the alloy Nb-Mo-Cr-Ti-Al and the alloy Nb-Mo-Cr-Ti-Al-1Si is hardly possible because these two alloys seem to essentially form the same oxides and the differences of the oxide mass fractions are rather small and therefore not meaningful. Nevertheless, some important conclusions can be drawn from the quantitative XRD analysis. Figure 9 shows the lattice parameters rutile identified using Rietveld analysis on powdered oxide scales formed on alloys Nb-Mo-Cr-Ti-Al (designated as “Nb” in Fig. 9) and Nb-Mo-Cr-Ti-Al-1Si (designated as “Nb1Si” in Fig. 9) after different oxidation times at 1000°C . It is obvious that the lattice parameters determined from samples of both alloys oxidized for 24h and 48h are almost identical. A slight deviation was only observed for the Si-free alloy oxidized for 8 h at 1000°C . This difference might be explained by the supposition that the initially formed rutile compound has not yet reached equilibrium. Further, Fig. 9 reviews literature data on lattice parameters of pure TiO_2 (designated as “ TiO_2 ”) [40-47], TiO_2 with Nb substituting Ti sites (designated as “ $\text{Ti}_{1-x}\text{Nb}_x\text{O}_2$ ”) [48, 49] as well as TiO_2 with Nb and Al substituting Ti (designated as “ $\text{Ti}_{0.6}\text{Al}_{0.2}\text{Nb}_{0.2}$ ”) [50]. Comparing the lattice parameter determined for rutile in this study with the literature data, it can be concluded that a certain amount of Nb may be dissolved in the rutile formed during oxidation of both alloys causing a significant cell distortion towards higher lattice parameters compared to pure TiO_2 . Considering that both Nb and Al can occupy Ti sites in rutile, it cannot be excluded that Al may also be dissolved in the rutile formed on the HEAs studied.

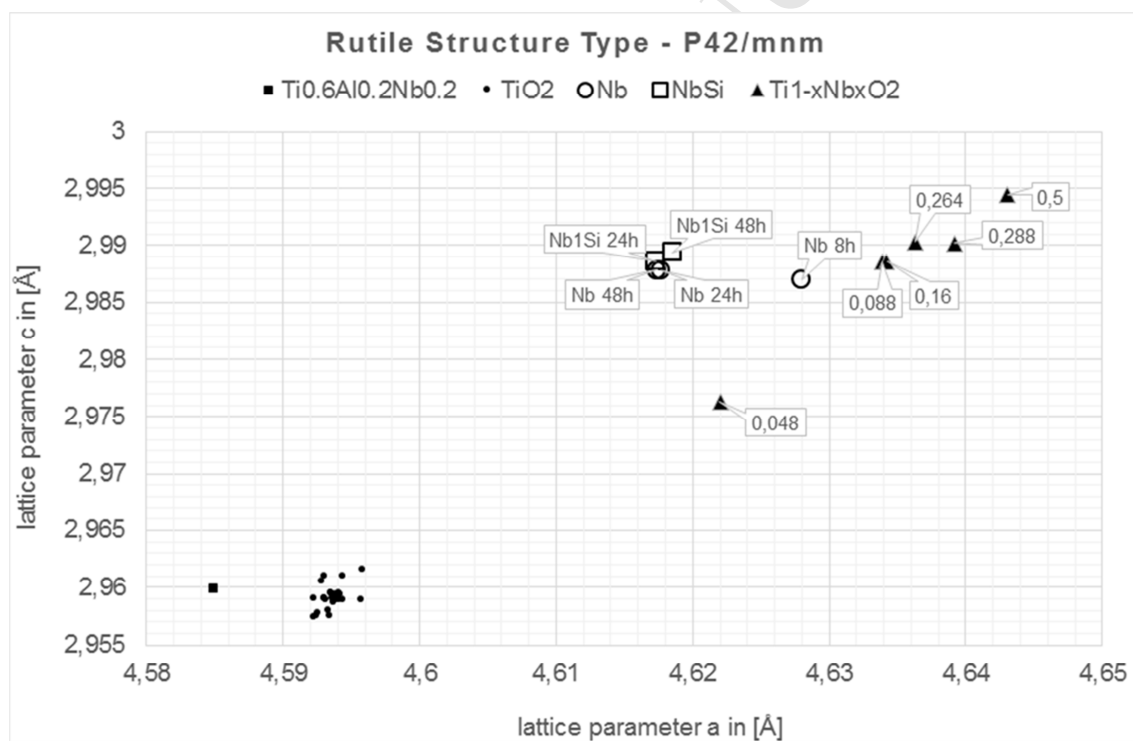


Figure 9: Lattice parameters of the rutile lattice structure identified in powdered oxide scales formed on the alloys Nb-Mo-Cr-Ti-Al (marked as open circle) and Nb-Mo-Cr-Ti-Al-1Si (marked as open square) after different oxidation times at 1000°C as well as literature data for pure TiO_2 (marked as point), $\text{Ti}_{1-x}\text{Nb}_x\text{O}_2$ (marked as filled triangle) and $\text{Ti}_{0.6}\text{Al}_{0.2}\text{Nb}_{0.2}$ (marked as filled square). References are given in text.

As relatively thick oxide scales were observed on the surface of both alloys, the dominant contribution to the mass gain of the alloys studied can obviously be attributed to the oxygen uptake through the formation of external oxide scales. It is well-known that the growth rate of pure chromia and α -alumina forming a dense layer is very slow and consequently low values of the parabolic oxidation

constants are reported in the literature, e.g. $2 \times 10^{-11} \text{ mg}^2 \text{ cm}^{-4} \text{ s}^{-1}$ for chromia and $7 \times 10^{-12} \text{ mg}^2 \text{ cm}^{-4} \text{ s}^{-1}$ for α -alumina [51] at 1000°C . During exposure to air at temperatures above approximately 800°C , pure Mo and Mo-based alloys form gaseous oxides that evaporate [52]. In case of the alloys investigated in this study, the evaporation of Mo oxides is presumably restricted to the initial transient oxidation stage, if it takes place at all. After a longer time of oxidation this effect can be neglected, since a clear Mo enrichment was observed at the interface oxide/substrate. It has been reported in the literature that both, Ti [53] and Nb [54], oxidize at 1000°C according to the linear rate law that is usually typical of the growth of non-protective surface scales. The linear oxidation constants of Ti and Nb are $0.013 \text{ mg cm}^{-2} \text{ min}^{-1}$ [53] and $1 \text{ mg cm}^{-2} \text{ min}^{-1}$ [54], respectively. As oxides of these two elements may possess the same rutile structure (see above) that was identified as the predominant phase, the oxidation of Ti and Nb seem to primarily account for the formation of the thick oxide scales. However, the relatively high mass gain during oxidation in air can also be attributed to a nitrogen uptake forming the nitrides TiN, Cr_2N and Nb_2N , which were experimentally identified in the thick zone of internal corrosion in the alloy Nb-Mo-Cr-Ti-Al exposed to air for 48h at 1000°C . Similar findings hold true for the alloy Nb-Mo-Cr-Ti-Al-1Si. Thick and porous oxide mixtures can form on the alloy surface if the oxides constituting the scale possess similar thermodynamic stabilities, such as Al_2O_3 and TiO_2 [46]. In order to assess the thermodynamic stability of the most relevant oxides in this alloy system, the standard free energies of formation of the possible oxides at 1000°C were calculated using the commercial software FactSage. The calculations were carried out assuming the element activities being equal unity. The calculated values of the standard free energy can however be considered since all elements in the alloys possess the same concentrations. The numbers are summarized in Table 3. In addition to the well-known similar thermodynamic affinity of oxygen to Al and Ti [55], almost identical values of the standard free energy of formation can be found for Nb_2O_5 and Cr_2O_3 . It can be assumed that the formation of a pure alumina on the alloy surface is retarded because of similar thermodynamic stability of Al_2O_3 and TiO_2 , while the formation of chromia is hampered because of the nearly equal values of the standard free energy for Nb_2O_5 and Cr_2O_3 . Probably due to the slightly higher thermodynamic stability of TiO_2 in the rutile modification as compared to anatase, the latter was detected by the XRD analysis only after 8h of oxidation as a transient phase. In terms of the thermodynamic stability of oxides listed in table 3 it can be concluded that all oxides, except MoO_3 , exhibit apparently high affinity to oxygen. Considering the very high oxidation rates of Ti and Nb discussed above, the predominant formation of the rutile phase consisting of Nb_2O_5 and TiO_2 becomes reasonable.

Table 3: Standard free energies of formation of oxides at 1000°C

oxide	Al_2O_3	TiO_2 (rutile)	TiO_2 (anatase)	Nb_2O_5	Cr_2O_3	MoO_3
ΔG^0 [kJ/mole O_2]	-853	-713	-702	-540	-538	-293

The values of standard free energies of formation of relevant nitrides at 1000°C are summarized in Table 4. As described above, three types of nitrides, i. e. TiN, Nb_2N and Cr_2N , were identified experimentally in the outer zone of internal corrosion of the alloy Nb-Mo-Cr-Ti-Al after air exposure for 48h at 1000°C . As shown in Table 4, Nb and Cr can form two corresponding types of nitrides, in each case the most stable one (Nb_2N , Cr_2N) was detected using XRD. It is also not surprising that TiN as the most stable nitride in this alloy system was identified in the inner zone of internal corrosion.

Table 4: Standard free energies of formation of nitrides at 1000°C

nitrides	TiN	AlN	Nb_2N	NbN	Cr_2N	CrN
ΔG^0 [kJ/mole N_2]	-434	-359	-251	-229	-64	-41

In terms of the high temperature oxidation resistance, the results presented here show the high potential of the new refractory HEAs. It is obvious that the oxidation behavior of these alloys can be moderately improved by micro-alloying, e.g. by Si, as was shown in this study. An increase of the Si concentration in the alloy Nb-Mo-Cr-Ti-Al up to 2-3 at.% may lead to a further improvement of oxidation resistance. However, the strongest effect on the oxidation behavior can certainly be achieved by macro-alloying, i.e. by substituting of some elements, for example Nb, in the alloy's chemical composition. The development of the new refractory HEAs primarily aims at the definition of a core alloy system providing the best combination of mechanical properties, ductility, and oxidation resistance. Hence, in our further studies, the effect of macro-alloying will be investigated and discussed by comparing the oxidation behavior of the alloy systems Nb-Mo-Cr-Ti-Al, W-Mo-Cr-Ti-Al, and Ta-Mo-Cr-Ti-Al.

Summary

In this study, high temperature oxidation behavior of the equiatomic refractory high-entropy alloy Nb-Mo-Cr-Ti-Al was investigated. The effect of 1 at.% of Si addition was also studied. The results can be summarized as follows.

1. Although the alloy 20Nb-20Mo-20Cr-20Ti-20Al contains a high amount of refractory elements, moderate mass gain was measured during oxidation in air. The oxidation kinetics follows the linear rate law at 900°C and 1000°C, while the decelerating oxidation rate was observed after approximately 30h at 1100°C. The metal surface was largely covered by thick, porous and non-protective oxide scales consisting of a mixture of various oxides. Localized, a relatively thin and more protective scale was observed containing an intermediate, semi-continuous Cr oxide-rich layer. At higher temperatures, an additional Al oxide-rich scale was identified after a prolonged oxidation time. A pronounced zone of internal corrosion was observed at all temperatures. The quantitative XRD analysis showed that rutile is the predominant phase in the oxide scale formed at 1000°C.
2. The addition of 1 at.% Si to the alloy 20Nb-20Mo-20Cr-20Ti-20Al improves the oxidation behavior moderately. The mass gain of the Si-containing alloy is by trend significantly lower compared to the Si-free alloy. The oxidation kinetics obeys the parabolic rate law up to approximately 30h and changes subsequently towards a linear oxidation rate. The Si-containing alloy largely forms the quite thin and compact oxide scale at 1000°C and 1100°C that contains nearly continuous and compact Cr- and Al-rich oxide layers. Thick and rather porous scales were predominantly observed on the sample corners. The moderate mass gain during oxidation and formation of the relatively thin oxide scale is mainly attributed to the formation of an Al-rich oxide layer. However, zones of internal corrosion were observed in all oxidized samples.
3. Though the HEAs represent a new material class, they show a high potential in terms of possible high temperature applications. The results of this investigation indicate that the oxidation behavior of these materials can be substantially improved by macro- and micro-alloying.

Acknowledgment The financial support by the Deutsche Forschungsgemeinschaft (DFG) is gratefully acknowledged.

References

- [1] Y. Zhang, T.T. Zuo, Z. Tang, M. Gao, K.A.Dahmen, P.K. Liaw, Z.P. Lu: Microstructure and properties of high-entropy alloys, *Progress in Materials Science*, 61 (2014) 1-93
- [2] M.C. Gao, C.S. Carney, Ö.N. Dogan, P.D. Jablonski, J.A. Hawk, D.E. Alman: Design of refractory high-entropy alloys, *JOM*, 67 (2015) 2653-2669
- [3] S. Guo, C.T. Liu: Phase stability in high entropy alloys: Formation of solid-solution phase or amorphous phase, *Progress in Natural Science: Materials International*, 21 (2011) 433-446
- [4] C.J. Tong, M.R. Chen, S.K. Chen, J.W. Yeh, T.T. Shun, S.J. Lin, S.Y. Chang: Mechanical performance of the AlCoCrCuFeNi high-entropy alloy system with multiprincipal elements, *Metallurgical and Materials Transactions A*, 36A, (2005) 1263-1271
- [5] J.W. Yeh, Y.L. Chen, S.J. Lin, S.K. Chen: High-entropy alloys – a new era of exploitation, *Materials Science Forum*, 560 (2007) 1-9
- [6] K.Y. Tsai, M.H. Tsai, J.W. Yeh: Sluggish diffusion in Co-Cr-Fe-Mn-Ni high entropy alloys, *Acta Materialia*, 61 (2013) 4887-4897
- [7] D.L. Beke, G. Erdelyi: On the diffusion in high-entropy alloys, *Materials Letters*, 163 (2016) 111-113
- [8] K.C. Hsieh, C.F. Yu, W.T. Hsieh, W.R. Chiang, J.S. Ku, J.H.Lai, C.P.Tu, C.C.Yang: The microstructure and phase equilibrium of new high performance high-entropy alloys, *Journal of Alloys and Compounds*, 483 (2008) 209-212
- [9] W.H. Liu, Y. Wu, J.Y. He, J. Y. Zhang, C.T. Kuz, Z.P. Lu: The phase competition and stability of high-entropy alloys, *JOM*, 66 (2014) 1973-1983.
- [10] A.J. Zaddach, C. Niu, C.C. Koch, and D.L. Irving: Mechanical properties and stacking fault energies of NiFeCrCoMn high-entropy alloys, *JOM* 65 (2013) 1780-1789
- [11] B. Gludovatz, E.P. George, R. Ritchie: Processing, microstructure and mechanical properties of the CrMnFeCoNi high-entropy alloy, *JOM* 67 (2015) 2262-2270
- [12] O.N. Senkov, C. Woodward, D.B. Miracle: Microstructure and properties of aluminium-containing refractory high-entropy alloys, *JOM*, 66 (2014) 2030-2042
- [13] P.K. Huang, J.W. Yeh, T.T. Shun, and S.K. Chen: Multi-principal-element alloys with improved oxidation and wear resistance for thermal spray coating, *Advanced Engineering Materials*, 6 (2004) 74-78
- [14] H.M. Daoud, A.M. Manzoni, R. Völkl, N. Wanderka, U. Glatzel: Oxidation behavior of Al₁₈Co₁₇Cr₁₇Cu₈Fe₁₇Ni₃₃, Al₂₃Co₁₅Cr₂₃Cu₈Fe₁₅Ni₁₅, and Al₁₇Co₁₇Cr₁₇Cu₁₇Fe₁₇Ni₁₇ compositionally complex alloys (high-entropy alloys) at elevated temperature in air, *Advanced Engineering Materials*, 17 (2015) 1134-1141
- [15] T.M. Butler, J.P. Alfano, R.L. Martens, M.L. Weaver: High-temperature oxidation behavior of Al-Co-Cr-Ni-(Fe or Si) multicomponent high-entropy alloys, *JOM*, 67 (2014) 246-259
- [16] S.T. Chen, W.Y. Tang, Y.F. Kuo, S.Y. Chen, C.H. Tsau, T.T. Shun, J.W. Yeh: Microstructure and properties of age-hardenable Al_xCrFe_{1.5}MnNi_{0.5} alloys, *Materials Science &*

- Engineering A: Structural Materials: Properties, Microstructure and Processing, 527 (2010) 21-22
- [17] T.M. Butler, M.L. Weaver: Oxidation behavior of arc melted AlCoCrFeNi multi-component high-entropy alloys, *Journal of Alloys and Compounds*, 674 (2016) 229-244
- [18] M.H. Chuang, M.H. Tsai, W.R. Wang, S.J. Lin, J.W. Yeh: Microstructure and wear behavior of Al_xCo_{1.5}CrFeNi_{1.5}Ti_y high-entropy alloys, *Acta Materialia*, 55 (2011) 6308-6317
- [19] J.C. Jiang, X.Y. Luo: High temperature oxidation behavior of AlCuTiFeNiCr high-entropy alloy, *Advanced Materials Research*, 652/654 (2013) 1115-1118
- [20] G. R. Holcomb, J. Tylczak, C. Carney: Oxidation of CoCrFrMnNi high entropy alloys, *JOM*, 67 (2015) 2326-2339
- [21] H.H. Yang, W.T. Tsai, J.C. Kuo: Effecto of pre-oxidation on increasing resistance of Fe-Al-Ni-Cr-Co-Mn high entropy alloys to molten Al attack, *Corrosion Engineering, Science and Technology*, 49 (2014) 124-129
- [22] O.N. Senkov, S.V. Senkova, D.M. Dimiduk, C. Woodward, D.B. Miracle: Oxidation behavior of a refractory NbCrMo_{0.5}Ta_{0.5}TiZr alloy, *Journal of Material Science*, 47 (2012) 6522-6534
- [23] Liu, C.M., Wang, H.M., Zhang, S.Q., Tang, H.B., Zhang, A.L.: Microstructure and oxidation behavior of new refractory high entropy alloys, *Journal of Alloys and Compounds*, 583 (2014) 162-169
- [24] C. Huang, Y. Zhang, J. Shen, R. Vilar: The stability and oxidation resistance of laser clad TiVCrAlSi high entropy alloy coating on Ti-6Al-4V alloy, *Surface & Coating Technology*, 206 (2011) 1389-1395
- [25] Gorr, B., Azim, M., Christ, H.-J., Mueller, T., Schliephake, D., Heilmaier, M.: Phase equilibria, microstructure, and high temperature oxidation resistance of novel refractory high-entropy alloys, *Journal of Alloys and Compounds*, 624 (2015) 270-278
- [26] Gorr, B., Azim, M., Christ, H.-J., Chen, H., Szabo, D.V., Kauffmann, A., Heilmaier, M.: Microstructure evolution in a new refractory high-entropy alloy, *Metallurgical and Materials Transaction*, 47A (2016) 961-970
- [27] H. Chen, A. Kauffmann, B. Gorr, D. Schliephake, C. Seemüller, J.N. Wagner, H.-J. Christ, M. Heilmaier: Microstructure and mechanical properties at elevated temperatures of a new Al-containing refractory high-entropy alloy Nb-Cr-Ti-Al, *Journal of Alloys and Compounds*, 661 (2016) 206-215
- [28] M. Horn, C.F. Schwerdtfeger, E.P. Meagher: Refinement of the structure of anatase at several temperatures, *Zeitschrift für Kristallographie* 136 (1972) 273-281
- [29] S. Kondo, K. Tateishi, N. Ishizawa: Structural evolution of corundum at high temperatures, *Japanese Journal of Applied Physics*, 47 (2008) 616-619
- [30] W.H. Baur, A.A. Khan: Rutile-type compounds, IV. SiO₂, GeO₂ and a comparison with other rutile-type structures, *Acta Crystallographica Section B*, B27 (1971) 2133-2139
- [31] D.E. Sands: Introduction to crystallography, Dover, New York, 1993

- [32] J. Novotny: Oxide semiconductors for solar energy conversion: titanium dioxide, CRC Press, 2011
- [33] F. Bondioli, A.M. Ferrari, C. Leonelli, Manfredini, L. Linati, P. Musterelli: Reaction mechanism in alumina/chromia (Al_2O_3 - Cr_2O_3) solid solution obtained by coprecipitation, *Journal of the American Ceramic Society*, 83 (2000) 2036-2040
- [34] Liu, Y., Weo, W., Benum, L., Oballa, M., Gyorffy, M., Chen, W.: Oxidation behavior of Ni-Cr-Fe-based alloys: Effect of alloy microstructure and silicon content, *Oxidation of Metals*, 73 (2010) 207-218
- [35] Evans, H.E., Hilton, D.A., Holm, R.A., Webster, S.J.: Influence of silicon additions on the oxidation resistance of a stainless steel, *Oxidation of Metals*, 19 (1983) 1-18
- [36] M. Heilmaier, M. Krüger, H. Saage, J. Rösler, D. Mukherji, U. Glatzel, R. Völkl, R. Hüttner, G. Eggeler, Ch. Somsen, T. Depka, H.-J. Christ, B. Gorr, S. Burk: Metallic materials for structural applications beyond nickel-based superalloys, *JOM* 61 (2009) 61-67.
- [37] Durcham, R., Gleeson, B., Young, D.J.: Silicon contamination effects in the oxidation of carbide-containing cobalt-chromium alloys, *Materials and Corrosion*, 49 (1998) 855-863
- [38] Wang, S., Wu, Y., Gesmundo, F., Niu, Y.: The effect of Si additions on the high temperature oxidation of a ternary Ni-10Cr-4Al alloy in 1atm O_2 at 900-1000°C, *Oxidation of Metals*, 69 (2008) 299-315
- [39] M. Schuetze, Die Korrosionswirkung oxidischer Deckschichten unter thermisch-chemisch-mechanischer Werkstoffbeanspruchung, Gebueder Borntraeger, Berlin, Stuttgart, 1991
- [40] W.H. Baur, A.A. Khan: Rutile-type compounds. VI. SiO_2 , GeO_2 and a comparison with other rutile-type structures, *Acta Crystallographica B* (24, 1968-38, 1982) 27 (1971) 2133-39
- [41] W.H. Baur: Über die Verfeinerung der Kristallstrukturbestimmung einiger Vertreter des Rutiltyps: TiO_2 , SnO_2 , GeO_2 und MgF_2 , *Acta Crystallographica* (1, 1948-23, 1967) 9 (1956) 515-520
- [42] S.C. Abrahams, J.L. Bernstein: Rutile: Normal probability plot analysis and accurate measurement of crystal structure, *Journal of Chemical Physics*, 55 (1971) 3206-3211
- [43] W.H. Baur: Atomabstände und Bindungswinkel im Rutil, *Naturwissenschaften*, 42 (1955) 295-296
- [44] H. Seki, N. Ishizawa, N. Mizutani, M. Kato: High temperature structure of the rutile-type oxides, TiO_2 and SnO_2 , *Journal of the Ceramic Association of Japan*, 92 (1984) 219-223
- [45] R. Restori, D. Schwarzenbach, J.R. Schneider: Charge density in rutile, TiO_2 , *Acta Crystallographica, Section B: Structural Science*, 43 (1987) 251-257
- [46] J.K. Burdett, T. Hughbanks, G.J. Miller, J.W. Richardson, J.V. Smith: Structural-electronic relationships in inorganic solids: Powder neutron diffraction studies of the rutile and anatase, *Journal of the American Chemical Society*, 109 (1987) 3639-3646
- [47] D.M. Tobaldi, A. Tucci, A. Sever Skapin, L. Esposito: Effects of SiO_2 addition on TiO_2 structure and photocatalytic activity, *Journal of the European Ceramic Society*, 30 (2010) 2481-2490

- [48] A. Peterson, H. Mueller-Buschmaum: Ein Beitrag über Oxide vom Typ AMO_4 ($A=Ti^{3+}$; $M=Nb^{5+}$, Ta^{5+}), *Zeitschrift für Anorganische und Allgemeine Chemie*, 609 (1992) 51-54
- [49] M. Okrusch, R. Hock, U. Schuessler, A. Brummer, M. Baier, H. Theisinger: Intergrown niobian rutile phases with Sc- and W-rich ferrocolumbite: an electron-microprobe and Rietveld study, *American Mineralogist*, 88 (2003) 986-995
- [50] I. Abrahams, P. G. Bruce, W.I.F. David, A.R. West: Structure determination of substituted rutiles by time-of-flight neutron diffraction, *Chemistry of Materials*, 1 (1989) 237-240
- [51] C.S Giggins, F.S. Pettit: Oxidation of Ni-Cr-Al alloys between 1000°C and 1200°C, *Journal of the Electrochemical Society*, 118 (1971) 1782-1790
- [52] E.A. Gulbransen, K.F. Andrew, F.A. Brassat: Oxidation of molybdenum 550° to 1700°C, *Journal of the Electrochemical Society*, 110 (1963) 110-119
- [53] P. Kofstad, P.B. Anderson, O.J. Krudtaa: Oxidation of Ti in the temperature range 800-1200°C, *Journal of Less Common Metals*, 3 (1961) 89-97
- [54] P. Kofstad, H. Kjollesdal: Oxidation of niobium (columbium) in the temperature range 500 to 1200°C, *Transaction of the Metallurgical Society of AIME*, 221 (1961) 285
- [55] S. Becker, A. Rahmel, M. Schorr, M. Schütze, Mechanism of isothermal oxidation of the intermetallic TiAl and of TiAl alloys, *Oxidation of Metals*, 38 (1992) 425-464

Highlights

- High temperature oxidation behavior of equimolar refractory alloys was studied.
- Inhomogeneous scales are formed on the alloy 20Nb-20Mo-20Cr-20Ti-20Al at 1000°C.
- The oxidation kinetics of the Si-free alloy follows the linear rate law.
- The addition of 1 at.% Si improves the oxidation resistance.
- Cr-rich and Al-rich oxide layers were found on the Si-containing alloy at 1000°C.